ARCHIVES OF MECHANICS
Arch. Mech. **76** (5), 451–470, 2024, DOI: 10.24423/aom.4514

Boundary layer tripping on a transonic compressor profile

A. JOSEPH*), M. PIOTROWICZ, P. FLASZYNSKI,
P. DOERFFER, P. KACZYNSKI

*Institute of Fluid-Flow Machinery, Polish Academy of Science (IMP PAN), Gdansk, Poland, e-mail**)*: ajoseph@imp.gda.pl (corresponding author)*

The numerical and experimental investigation of boundary layer tripping using steps on the suction side of a transonic compressor rotor has been presented in this paper. The presented research corresponds to an EU project known as TFAST (Transition Location Effects on Shock Wave Boundary Layer Interaction). A representative single passage test section has been designed to investigate the SBLI (Shock wave Boundary Layer Interaction) effects on the rotor profile. The geometrical and inflow boundary conditions have been defined by the project partner RRD (Rolls-Royce Deutschland). Two locations of step ($x/c = 0.16$ and $x/c = 0.02$) were chosen upstream of the shock location to investigate the boundary layer tripping effects and are compared with configuration without tripping setup. The numerical simulations were carried out on the test section model using the steady-state Reynolds Averaged Navier–Stokes (RANS) model with Explicit Algebraic Reynolds Stress Model (EARSM) turbulence model with transition effects included. The chosen turbulence model could accurately predict the shock location on the suction side of the lower profile in the test section and had a good agreement with wall pressure measurements using pressure taps. A detailed shock structure was captured using the schlieren technique and compared for different tripping configurations. To estimate the effectiveness of the tripping setup losses have been estimated using LDA (Laser Doppler Anemometry) along the traverse downstream the blade passage. To understand the tripping effect on the boundary layer a detailed investigation has been carried out at ten selected traverse locations from leading edge to trailing edge of the rotor profile. Based on the experimental validation of the defined numerical model for tripping setup, a few more step heights were compared at selected tripping locations numerically. To analyse the effect of step heights, the isentropic Mach number and wall shear stress are compared with without tripping configuration. The wake and stagnation pressure losses downstream of the profile have been compared to investigate the sensitivity of location and geometrical definition of the boundary layer tripping setup on the aerodynamic losses.

Key words: transonic aerodynamics, turbomachinery, internal flows, axial compressors, SBLI, flow control.

1. Introduction

The research on the Shock wave Boundary Layer Interaction (SBLI) remains an important topic of interest today due to its numerous applications in both external and internal aerodynamics. The flow structure of SBLI and its detrimental effect on transonic airfoils have been researched for decades. The aerodynamic performance of turbomachinery blading is strongly dependent on the nature of the boundary layer developed on the profiles [1]. The nature of SBLI critically depends on the boundary layer character (laminar or turbulent) in front of the shock wave [2]. Huge efforts were made with different applications to maintain the laminar boundary layer upstream of the normal shock to reduce drag caused by skin friction [3]. Due to this benefit, the laminar boundary layer is preferred as a drag-reducing design choice for wings and the low Reynolds number (Re) applications. At higher altitudes where Re drops to a factor of 4 compared to sea level conditions, it is relatively easier to maintain laminar flow. This gives low skin friction, which is desirable. However, the laminar boundary layer has the advantage of lower drag but is more sensitive to separation in adverse pressure gradients. This can lead to increased total pressure losses and flow unsteadiness in internal flows [4].

The interaction of the laminar boundary layer with a shock wave is more likely to induce separation, therefore a weaker shock can cause such an effect of interaction resulting in degradation of blade performance. The laminar SBLI should be avoided, especially when in some applications this interaction becomes unsteady and may induce shock oscillation in internal flows [5]. Therefore, the transition to a turbulent boundary layer should take place before shock interacts with the boundary layer. When compared to turbulent SBLI, laminar SBLI causes higher total losses and an increase in flow separation tendency [6, 7]. These effects are prominent at higher altitude conditions where the Reynolds number is significantly lower than at sea-level conditions. Considering the benefits of the laminar boundary layer, the transition location should be delayed as much as possible. The laminar/transitional/turbulent SBLIs become especially complex when unsteadiness takes place in internal flows. The real challenge is in locating the transition position closest to the shock wave while ensuring that the interaction is of turbulent type, meaning that it has the least amount of adverse pressure effects such as separation, unsteadiness, and large shock lambda foot. The use of flow control applications in turbomachinery has the potential to break down fundamental barriers [8].

Flow control methods can be subdivided into active and passive methods depending on whether they require additional energy or not. Investigation of Active Flow Control (AFC) with compressor blade instabilities, boundary layer separation, and secondary flow structures are detailed in [9–12]. Instead, passive flow control methods do not require any additional energy source to operate compared to AFC. The advantages of passive flow control methods, described in [13–15], include lift augmentation, drag reduction, reduced tip leakage flows, and separation control. Many passive flow control methods like roughness patches, riblets, tripping devices, etc. have been discussed in the literature [11, 16, 17].

To induce transition in the boundary layer, various tripping devices can be used. One of the boundary layer tripping methods chosen for investigation in this paper, is to introduce a small step upstream of the shock wave. The research presented in this paper was a part of the EU-TFAST (Transition Location Effect on Shock Wave Boundary Layer Interaction) project and some of the numerical and experimental research on this topic has already been published [18].

The general objective of this project was to improve the knowledge of laminar SBLI and to study the effect of transition location on the structure of interaction between a shock wave and a boundary layer. To investigate the SBLI effects numerically and experimentally on the compressor rotor, a single passage test section with two profiles has been designed for the IMP PAN transonic wind tunnel facility. To avoid the laminar SBLI, the boundary layer has been tripped using a passive flow control method of step defined on the suction side of the profile. The effectiveness of boundary layer tripping based on different step locations has been briefly described in this paper. A detailed flow structure comparison has been presented in this paper with chosen cases ($x/c = 0.02$ as turbulent), ($x/c = 0.16$ as transitional), and without (laminar) tripping setup on the suction side of the lower profile in the test section. Based on these findings further investigation has been carried out to investigate the influence of different step heights on boundary layer tripping. This research aims to extend the knowledge beyond what was obtained in the TFAST project.

2. Experimental setup

The experimental investigations were carried out at the transonic wind tunnel facility of the Institute of Fluid Flow Machinery, Polish Academy of Sciences (IMP PAN). For investigating the SBLI effects numerically and experimentally, anew cascade geometry has been designed by a partner of the EU-TFAST project Rolls-Royce Deutschland (RRD). The geometrical parameters of the designed cascade are listed in Table 1.

To carry out an experimental investigation on the delivered cascade, a rectilinear single passage test section has been designed based on the streamlines extracted from the cascade simulations. Such an approach has been proven effective in the previous studies carried out at the IMP PAN facility. The inlet Mach number and inflow stream uniformity are two design criteria that are considered while designing the test section. The major challenge in designing the test section is to reproduce a similar flow structure as in cascade simulations at the blade suction side. The relative location of blades in the test section is defined as a cascade configuration. An inlet nozzle design has been designed upstream of the profiles to maintain the flow uniformity upstream of the profiles and to achieve the required inlet Mach number of $\mathrm{M} = 1.22$. The single passage

TABLE 1. Geometrical description of delivered cascade profile.

Parameters	Units	Values
Inlet Mach number	–	1.22
Chord length	mm	100
Pitch to chord ratio	–	0.60
Thickness to chord ratio	–	0.03
Blade inlet angle	deg	50.90
Blade exit angle	deg	33.20
Flow inlet angle	deg	55.50
AVDR	–	1.23

test section designed for SBLI investigations on the lower profile suction side is shown in (Fig. 1). Whenever the 'suction side' is mentioned in this paper it refers to the lower blade. The profiles are mounted using supporting structures rather than fastened to sidewalls because of the advantage of the profile position adjustment rather than a fixed location at sidewalls which are made of glass windows. Additionally, an AFC method of suction slots has been introduced in the test section. There are two sets of suction slots defined in the test section for different purposes. The first set includes slots that are placed at lower and upper limiting walls, respectively (Fig. 1). Their purpose is to control the possible flow blockage in passages below the lower and above the upper profile to control boundary layer thickness and to achieve the supersonic conditions upstream of the profiles. A detailed description of these slots in the test section has been described in [19]. The second set of suction slots is placed at both supports of the blade close to the sidewall. These suction slots help in the reduction of corner flows developed between the blade and sidewall resulting in the control of AVDR in the test section.

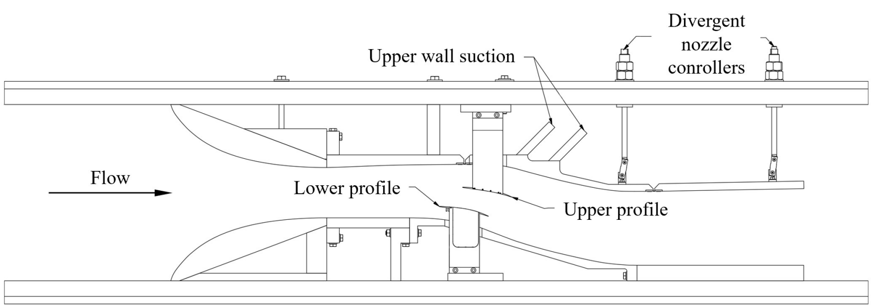

FIG. 1. Schematic drawing of test section in IMP PAN transonic windtunnel facility.

A detailed investigation of the suction slot effect on the suction side of the profile has been briefly described in [20]. The test section's mass flow and flow structure can be controlled and modified by adjusting the static pressure at the suction slots, hence the suction mass flow rate. The static pressures are measured upstream of the blade passage and at the mid-span location of the blade suction side, which accounts for 46% of the overall chord length. The location and structure of the shock wave have been captured with a *Canon EOS M50* camera and the z-coordinate schlieren setup. To estimate the inflow turbulence and wake downstream the blade passage the Laser Doppler Anemometry (LDA) measurement technique has been used. A *Coherent Innova 70C 5W* argon-ion laser with beam wavelengths of 514.4 nm and 488 nm is used as the laser source, and the laser beam is split using a *Fiber Flow System* from *Dantec Dynamice*. The *Flow Tracker 700 CE* uses DEHS (*Di-Ethyl-Hexyl-Sebacic*) oil with an average particle size of 2 μm to create the seeding particles.

Geometrical definition of boundary layer tripping setup

This paper investigates the passive flow control method using boundary layer tripping by a defined step on the suction side of the transonic fan profile. Built upon the investigations carried out on the profile in the test section the boundary layer upstream of the shock wave is laminar and the interaction of the shock wave with the boundary layer is laminar SBLI without any transition control, referred as **Clean** configuration. To force the transition two different locations of the tripping setup (**Step 1** at $x/c = 0.16$ and **Step 2** at $x/c = 0.02$) on the suction side of the profile have been chosen and the results are compared with the **Clean** case. The geometrical definition of the step has been defined in Table 2. The step has been created using a tape stuck to the profile with the defined length and width extending over the whole blade span-wise length of 100 mm.

Table 2. The geometrical definition of boundary layer tripping step.

Configuration	Width [mm]	Height [mm]
Clean	–	–
Step 1 ($x/c = 0.16$)	5.00	0.10
Step 2 ($x/c = 0.02$)	2.50	0.40

3. Numerical model description

To investigate the SBLI effects on compressor rotor cascade, numerical investigations have been carried out on the test section model which has been designed corresponding to the cascade model. Numerical simulations were carried out using Numeca Fine/Turbo. The structured mesh was generated using IGG/Numeca as shown in (Fig. 2).

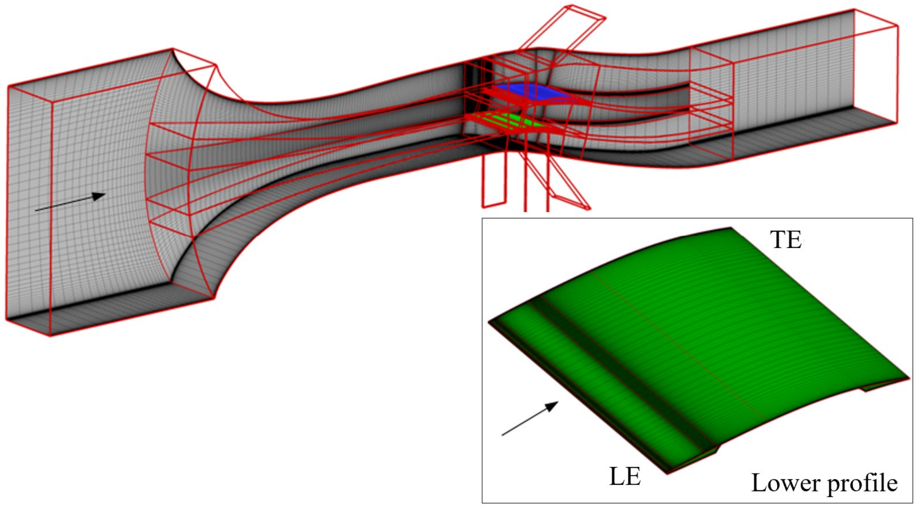

FIG. 2. Numerical model of test section with multi-block structured grid created using IGG, and the profile suction side is displayed in green color.

The multi-block topology consists of 35 blocks with a total number of hexahedral cells of 18.6×10^6. The resolution of mesh close to the wall is kept adequate to obtain y^+ of 1. The quality of the mesh has been checked to make sure that it is within the defined limit by the chosen turbulence model. The mesh quality parameters such as cell orthogonality expansion ratio and aspect ratios of the defined mesh domain have been quantified in Table 3.

TABLE 3. The quality parameters of the defined mesh domain.

Mesh parameter	Range	Percentage of cells [%]
Orthogonality	90–75°	90
	75–60°	9
	60–45°	1
Expansion ratio	1.0–1.1	43
	1.1–1.2	26
	1.2–1.3	30
	1.3–1.4	1
Aspect ratio	1–330	97
	330–670	2
	670–1000	1

The 1% cells for the orthogonality range corresponds to the location where the greatest curvature of geometry is defined especially at the leading and trailing edges of the profiles. This numerical approach solves 3D Reynolds-averaged Navier–Stokes equations (RANS) using non-orthogonal multi-block grids. The RANS equations are simplified versions of the general Navier–Stokes equations. The Navier–Stokes equations are the fundamental governing equations for viscous, heat-conducting fluids. It is a vector equation generated by applying Newton's Law of Motion to a fluid element; it is also known as the momentum equation (3.1):

$$\frac{\partial}{\partial t}(\rho u_i) + \frac{\partial}{\partial x_j}[\rho u_i u_j + p\delta_{ij} - \tau_{ji}] = 0, \qquad i = 1, 2, 3, \tag{3.1}$$

where u is the flow velocity, ρ is the fluid density, p is the pressure, μ is the dynamic viscosity and τ is the viscous stress of the chosen fluid. It is supplemented by the mass conservation equation, also called continuity equation (3.2) and the energy equation (3.3):

$$\frac{\partial \rho}{\partial t} + \nabla \cdot (\rho u) = 0, \tag{3.2}$$

$$\frac{\partial}{\partial t}(\rho e_0) + \frac{\partial}{\partial x_j}[\rho u_j e_0 + u_j p + q_j - u_i \tau_{ij}] = 0, \tag{3.3}$$

where e_0 is the total energy and q_j is the heat flux for the given fluid. For the numerical simulations spatial discretization using the second-order central difference scheme with scalar artificial dissipation formulated by JAMESON and TURKEL [21] was applied. The Baseline Explicit Algebraic Reynolds Stress Model (BSL-EASRM), proposed by MENTER [22], is a two-equation nonlinear eddy viscosity turbulence model that extends the $k\omega$-SST turbulence model as shown in Eqs. (3.4) and (3.5):

$$\frac{D\rho k}{Dt} = \tau_{ij}\frac{\partial u_i}{\partial x_j} - \beta^* \rho \omega k + \frac{\partial}{\partial x_j}\left[(\mu + \sigma_k \mu_t)\frac{\partial k}{\partial x_j}\right], \tag{3.4}$$

$$\begin{aligned}\frac{D\rho\omega}{Dt} = \frac{\gamma}{\nu_t}\tau_{ij}\frac{\partial u_i}{\partial x_j} - \beta\rho\omega^2 + \frac{\partial}{\partial x_j}\left[(\mu + \sigma_\omega \mu_t)\frac{\partial \omega}{\partial x_j}\right] \\ + 2\rho(1 - F_1)\sigma_{\omega 2}\frac{1}{\omega}\frac{\partial k}{\partial x_j}\frac{\partial \omega}{\partial x_j},\end{aligned} \tag{3.5}$$

where k is the turbulent kinetic energy and ω is the specific dissipation rate. The coefficients $\beta = 3/40$, $\beta^* = 9/100$, $\sigma k = 0.85$ and $\sigma\omega = 0.5$ are the model constants. It has been decided to use the generalized transition model [23]. This model is defined on two transport equations, Eqs. (3.6) and (3.7), for the intermittency (γ) and the transition momentum thickness Reynolds number ($\tilde{\mathrm{Re}}_{\theta t}$)

$$\frac{\partial \rho\gamma}{\partial t} + \frac{\partial \rho u_j \gamma}{\partial x_j} = P_\gamma - E_\gamma + \frac{\partial}{\partial x_j}\left(\left(\mu + \frac{\mu_t}{\sigma_f}\right)\frac{\partial \gamma}{\partial x_j}\right), \tag{3.6}$$

$$\frac{\partial \rho \tilde{\mathrm{Re}}_{\theta t}}{\partial t} + \frac{\partial \rho u_j \tilde{\mathrm{Re}}_{\theta t}}{\partial x_j} = P_{\theta t} + \frac{\partial}{\partial x_j}\left(\sigma_{\theta t}(\mu + \mu_t)\frac{\partial \tilde{\mathrm{Re}}_{\theta t}}{\partial x_j}\right), \tag{3.7}$$

where P_γ and E_γ are the transition sources for intermittency whereas $P_{\theta t}$ and t are source terms for the momentum thickness Reynolds number. A perfect gas equation and Sutherland's law for viscosity complete the set of equations. Inlet boundary conditions have been defined with ambient conditions a total pressure of 101 kPa and a total temperature of 293 K. The boundary conditions for simulations have been defined upon the experiment. The turbulent intensity was defined as 0.8% according to the measurement carried out upstream of the profile. The viscosity ratio has been defined as 10 at the inlet. At the outlet, the boundary conditions have been defined with static pressure of 76 kPa to obtain the required shock wave location on the suction side of the profile.

4. Numerical and experimental results

The numerical and experimental investigations have been carried out for three cases: **Clean** – laminar SBLI, **Step 1** – transitional SBLI, and **Step 2** – turbulent SBLI. The inflow conditions defined by RRD, an the inlet Mach number of M = 1.22 has been maintained for all three cases. To investigate the shock structure in detail, an experimental schlieren with a vertical knife position has been compared with numerical schlieren formulated upon the density gradient magnitude as shown in (Fig. 3). The shock generated on the leading edge of the upper and lower profiles and the shock reflection from the upper wall are well captured in Fig. 3. The beginning of separation and stagnation zones are visible in schlieren images as oblique dark regions upstream close to the main shock wave. Whereas a thicker dark oblique zone is visible well upstream the main shock marked as lip shock showing the presence of an oblique shock presence. The main interest is in the shock generated at the leading edge of the upper profile interacting with the boundary layer at the profile.

For shock wave interaction with the laminar boundary layer, a significant distance typically exists between the interaction's onset and the main shock wave location. The effect of the tripping step is clearly visible in numerical schlieren for **Step 1** and **Step 2** cases shown in Fig. 3. The existence of compression and expansion waves is more pronounced at the upstream and downstream of the defined step geometry on the suction side. From Fig. 3, the size of λ-foot is comparable for cases with and without tripping setup. The static pressure measured at the mid-span of profile, the isentropic Mach number has been compared with and without the tripping case as shown in Fig. 4.

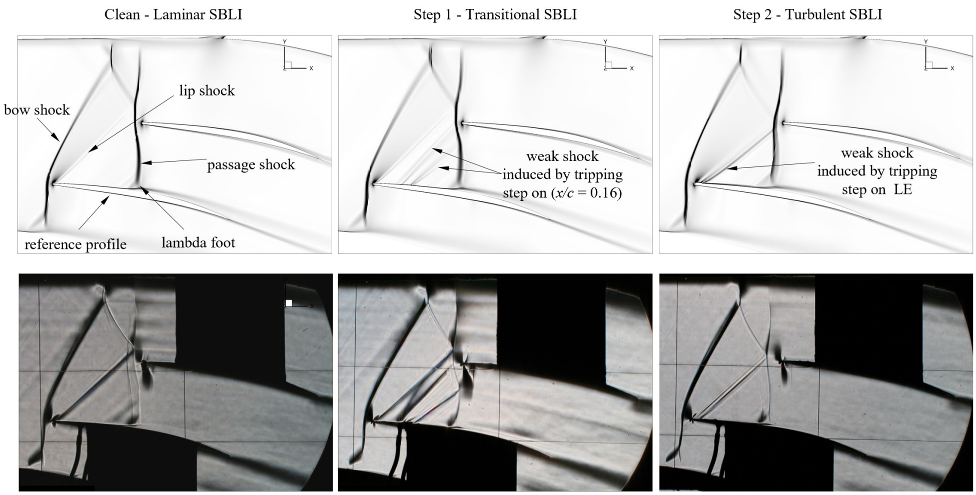

FIG. 3. Comparison of (above) numerical schlieren and (bottom) experimental schlieren visualization for three cases.

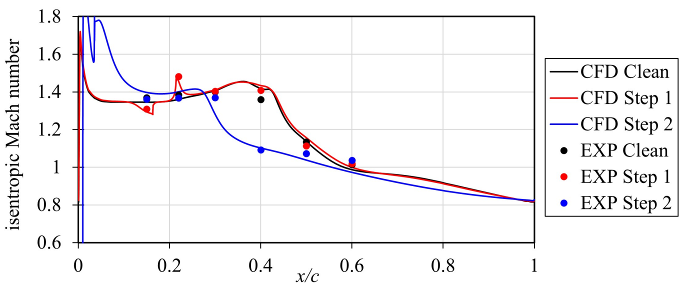

FIG. 4. Comparison of isentropic Mach number plotted along the suction side of profile in the test section.

From Fig. 4, it is evident that the chosen turbulence model could accurately predict the shock distribution on the profile. The spikes or disturbances visible in the isentropic Mach number plot for **Step 1** and **Step 2** are also seen in schlieren images, which correspond to the location of expansion and compression waves due to the tripping step. In the case of the isentropic Mach number distribution it can be seen that the shock wave is shifted slightly downstream the **Clean** case whereas the shock wave is shifted significantly upstream for **Step 2**. The difference in shock wave location is more pronounced till shock wave location and downstream the shock wave the differences between the cases are comparable. To investigate the flow structure in the test section, velocities have been measured at a different traverse location in the test section using LDA (Laser Doppler Anemometry) as shown in Fig. 5.

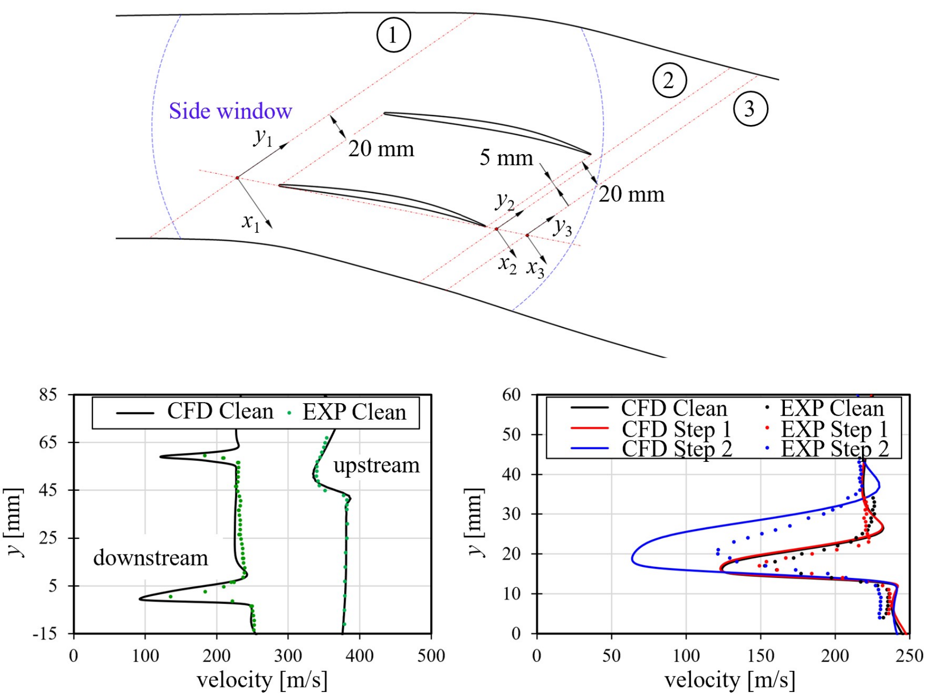

Fig. 5. (Top) Traverse location plotted upstream and downstream of the profiles at mid-span location in test section, (bottom) comparison of velocities for different configurations at (left) Traverse 2 and Traverse 1 (right) Traverse 3.

To evaluate the inflow conditions according to the requirement, velocity has been measured at the traverse located 20 mm upstream of the profiles and mid-span location in the test section as shown in Fig. 5. The experimental measurements have a good fit with numerical prediction at this location. The $(x, y = 0)$ traverse has been located upstream of the leading edge of the profile. There is a sudden decrease in the velocity plot at the upstream traverse at $(y = 50\,\text{mm})$ due to the intersection of leading-edge shock generated due to the profile. The distribution till $(y = 0$ to $y = 40\,\text{mm})$ depicts the uniform flow distribution upstream of the profiles. Inlet conditions in all three cases are identical, therefore the plots of the **Clean** case have only been shown in Fig. 5. Wake measurements can be used to assess the effect of the tripping device on the flow structure. The measurements are carried out at 5 mm and 20 mm downstream of the trailing edge of the profiles at the mid-span location and are shown in Fig. 5. The wake of the **Clean** case has been plotted at the traverse located 5 mm downstream of the trailing edge. The measurement data do not have points at the wake downstream of the lower and upper profile trailing edge because of the reduced seeding effect caused by the flow separation region closer to the trailing edge of the blades. Whereas further downstream traverse location of 20 mm could feed more seeding due to the higher dissipation effect of wake from boundary layer separation. Therefore, a 20 mm traverse downstream of the trailing edge was chosen for comparing the losses with or without a tripping setup as shown in Fig. 5. It is evident that the chosen numerical model overpredicts the wake thickness compared to experimental data, which gives scope of improvement in using high-order numerical models for such predictions.

On the other hand, the experiment carried out in the test section is too complex due to the flow mixing of unsteady flow from the pressure side of the lower blade with boundary layer separation from the suction side. This could also be a reason that the experimental prediction of wake is smaller and thinner than numerical predictions. From the wake, it is visible that **Clean** and **Step 1** cases have very similar wake thicknesses which translates to comparable losses. Whereas in **Step 2** due to overtripping the boundary layer is thicker which finally leads to a much wider wake. To compare the effects of the tripping device it is essential to investigate the boundary layer on the suction side of the profile in these cases. The boundary layer from the leading edge to the trailing edge at ten selected traverse locations has been compared and is plotted for compressible flow conditions in (Fig. 6).

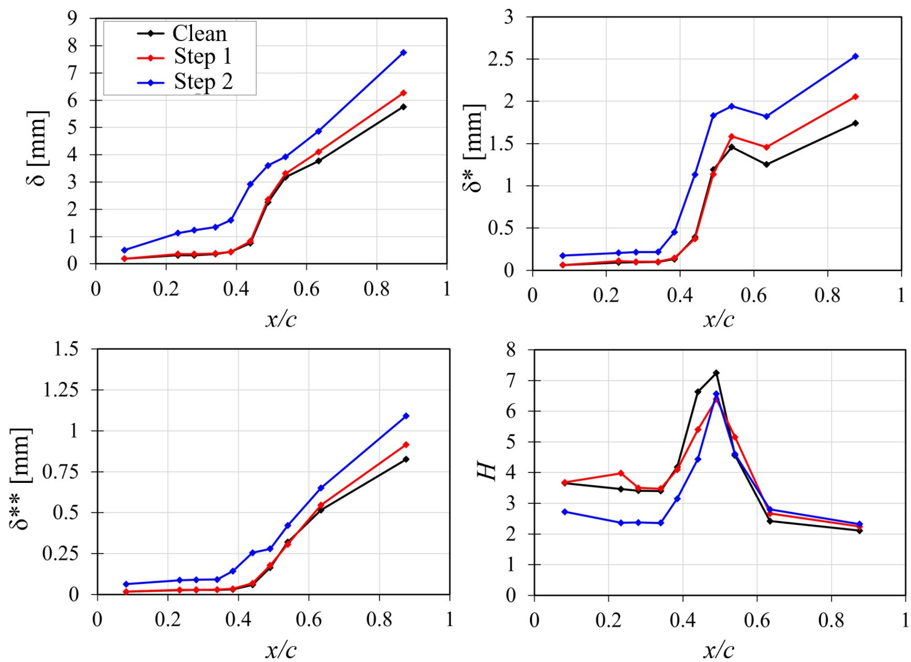

Fig. 6. Comparison of thickness and integral parameters of boundary layer.

According to the boundary layer thickness plot, **Clean** and **Step 1** cases have comparable boundary layer thickness up to $x/c = 0.53$. The boundary layer becomes thicker from the beginning of the separation bubble and continues to be separated from the surface. From the boundary layer thickness plot, it can be seen that the boundary layer tripping at **Step 1** has a very weak effect on the flow field and has a very similar boundary layer structure as in the laminar **Clean** case. Whereas in the **Step 2** case, the boundary layer is thicker from the leading edge to the trailing edge compared to the **Clean** and **Step 1** cases. According to the boundary layer thickness plot shown in (Fig. 6), **Step 2** overtrips the boundary layer resulting in a large separation which translates to higher losses. This aspect is also affirmed by the wake comparison shown in (Fig. 5). The displacement thickness plotted in (Fig. 6) shows a similar trend to boundary layer thickness. The differences are pronounced further downstream than the shock interaction locations. There is a steep increase upstream of the separation bubble and a drop in the displacement thickness at the reattachment zone visible in Fig. 6. The increase of displacement thickness continues further downstream in the reattachment zone. The momentum thickness plotted in Fig. 6 also follows a similar trend visible in the boundary layer plot. Another important aspect of the integral parameter of the boundary layer is the shape factor (H), which is estimated as the ratio of displacement thickness and momentum thickness. The shape factor is used to determine the nature of the flow. Conventionally, $H = 2.59$ is typically for the laminar boundary layer and $H = 1.3$ to 1.4 typical for the turbulent boundary layer [24].

This is applicable to the incompressible coefficient where density remains constant throughout the flow field. The shape factor has been estimated for the corresponding tripping cases for the compressible coefficient and incompressible coefficients and is plotted in (Fig. 7). The estimation in incompressible flow cases

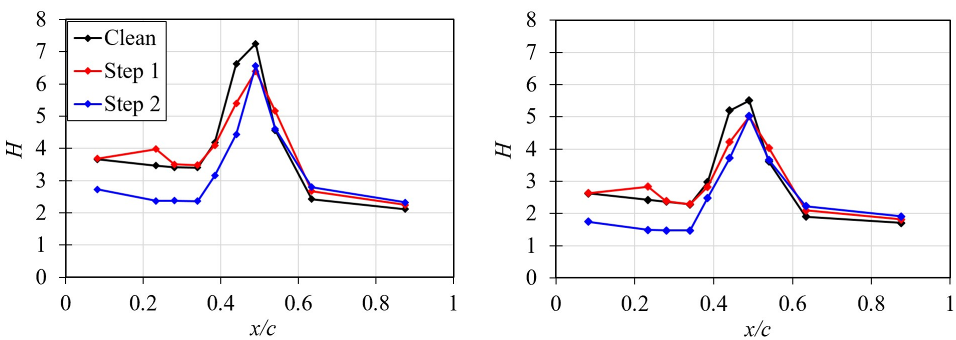

FIG. 7. Comparison of shape factor estimated using (left) compressible coefficient, (right) incompressible coefficient.

is carried out by maintaining constant density. From the shape factor it could be concluded that the **Clean** and **Step 1** cases have a laminar boundary layer ($H = 2.59$) up to ($x/c = 0.35$) where the separation bubble starts. The spike visible at ($x/c = 0.16$) for **Step 1** represents the step location on the suction side of the profile. **Step 1** has a very weak effect on tripping the boundary layer, whereas **Step 2** has a turbulent boundary layer from the leading edge ($H = 1.3$–1.4) till the beginning of the separation bubble. It is typical behavior in shape factor plots that the sudden spike corresponds to separation location and the drop in the shape factor to a plateau level shows the reattachment location on the surface. One could see that the separation starts at ($x/c = 0.35$) and reattaches at ($x/c = 0.65$) in all three cases. For **Clean** and **Step 1** downstream the reattachment of the boundary layer is in a transitional state ($H = 1.5$–2).

5. Numerical investigation of different step height

Additional investigations have been carried out numerically at **Steps 1** and **2** for various step heights to observe how they adhere to the tripping of the boundary layer according to the numerical and experimental investigation of boundary layer tripping presented in the previous section. The geometrical definition of this numerical configuration has been listed in Table 4.

Table 4. Geometrical definitions of tripping setup for different step heights.

Configuration	Location	Width [mm]	Height [mm]
Case 1a	Step 1 ($x/c = 0.16$)	5.00	0.05
Case 1b	Step 1 ($x/c = 0.16$)	5.00	0.10
Case 1c	Step 1 ($x/c = 0.16$)	5.00	0.40
Case 2a	Step 2 ($x/c = 0.02$)	2.50	0.05
Case 2b	Step 2 ($x/c = 0.02$)	2.50	0.40
Case 2c	Step 2 ($x/c = 0.02$)	2.50	0.80

The location and width of the step are identical to the configuration which has been investigated experimentally. The step heights have been chosen as one size smaller and one size larger than the experimental case which is **Case 1b** and **Case 2b.** The numerical investigation of three different step heights for **Step 1** configuration has been carried out on the suction side of the profile. The isentropic Mach number and wall shear stress for three-step heights of **Step 1** configuration have been compared with clean configuration and are plotted in Fig. 8. From the isentropic Mach number plot it is evident that **Case 1a** and **Case 1b** have a very similar shock structure and location as the **Clean** case on the suction side of the profile. Whereas **Case 1c** is overtripping the boundary

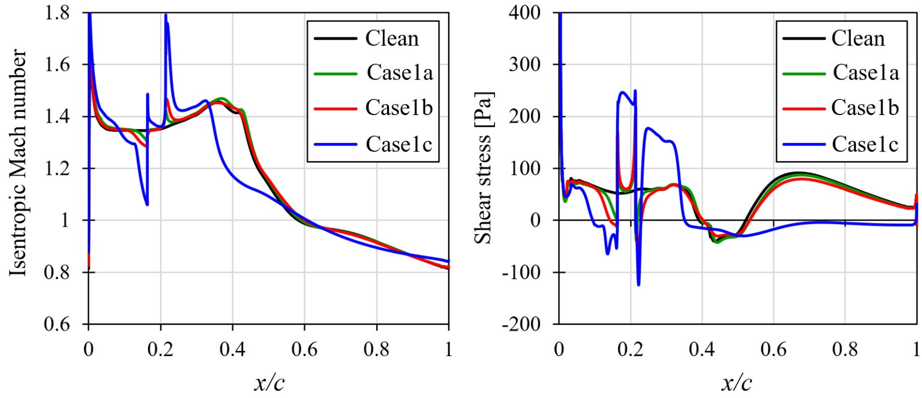

FIG. 8. Comparison of different step height for boundary layer tripping configuration. Step 1 ($x/c = 0.16$), (left) isentropic Mach number plot, (right) wall shear stress stress.

layer and the shock location is moved upstream. The spike in the isentropic Mach number at ($x/c = 0.16$) corresponds to the location of the tripping step. The shear stresses plotted on the suction side of the profile show the behavior of the boundary layer and the location of the separation bubble. The shear stresses are lower upstream, the shock interaction shows the boundary layer is laminar whereas the shear stresses are higher for **Case 1c** corresponding to the turbulent nature of the boundary layer. Therefore, **Case 1c** is over-tripping the boundary layer compared to **Cases 1a** and **1b**. Also, the separation starts significantly upstream for **Case 1c** compared to **Case 1a**, **1b**, and **Clean** cases and reattaches further downstream. It also depicts that the bubble height is very small in **Case 1c** in comparison to other cases. The flow separation is significantly higher and does not reattach up to the trailing edge for **Case 1c**. This shows the sensitivity of the step height at the $x/c = 0.16$ location. Similarly, it is important to investigate different step heights for turbulent SBLI case **Step 2**. As **Step 1**, three-step heights have been chosen to investigate the boundary layer tripping effect on the suction side of the profile. The isentropic mach number and wall shear stress for three different step heights of **Step 2** configuration have been compared with a clean configuration and are plotted in Fig. 9.

According to the isentropic Mach number plotted in (Fig. 9), **Case 2a** has a negligible effect on tripping the boundary layer and has an identical distribution of shock as of **Clean** case. Whereas the increasing of step heights from **Case 2a** to **Case 2b** and **2c** shows that the boundary layer is over-tripped, and the shock wave moves upstream corresponding to a step height increase. The wall shear stresses plotted in (Fig. 9) for **Step 2**, the location of the separation bubble for **Case 2a** is identical to the **Clean** case. Also, the shear stress is identical to the **Clean** case upstream of the shock wave which is the laminar boundary

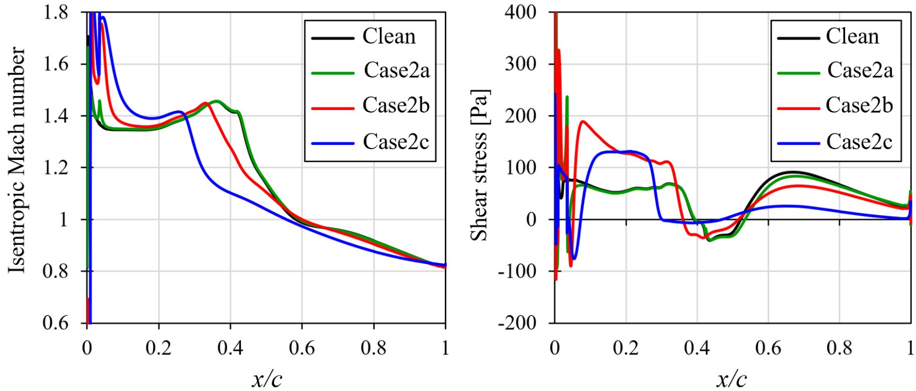

Fig. 9. Comparison of different step height for boundary layer tripping configuration. **Step 2** ($x/c = 0.02$), (left) isentropic Mach number plot, (right) wall shear stress stress.

layer. Whereas **Case 2b** and **2c** have overtripped boundary layers resulting in higher shear stresses upstream of the shock location. The location of the separation bubble which corresponds to the location of the shock wave is shifted upstream for **Case 2b** and **2c** cases. The height of the separation bubble is much smaller in **Case 2c** compared to other cases, whereas **Case 2b** has a comparable separation bubble height with **Clean** and **Case 2a** cases. Therefore, the step height is very sensitive to the tripping of the boundary layer close to the leading edge at ($x/c = 0.02$). To investigate the losses of the wakes downstream, the blade passage for the cases has been estimated and is plotted in (Fig. 10).

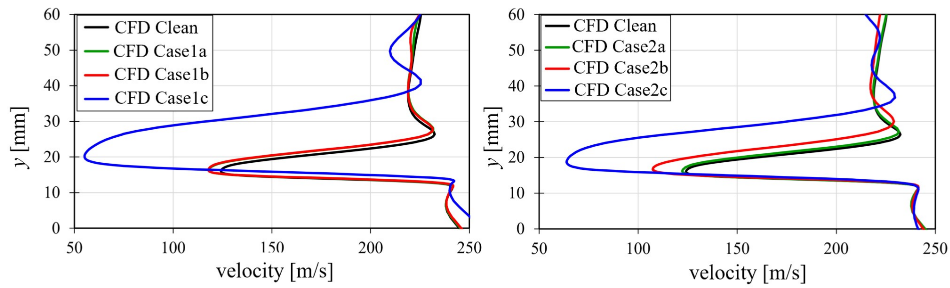

Fig. 10. Comparison of wake at traverse located 20 mm downstream the blade (left) different step heights for **Step 1** (right) different step height for **Step 2**.

The wakes compared at traverse located 20 mm downstream the blade trailing edge for **Step 1** shows that **Case 1a** and **Case 1b** have very similar thicknesses which corresponds to slightly higher losses compared to the laminar **Clean** case.

Whereas the increased height of the step for **Case 2c** has a significantly thicker wake which translates to higher losses compared to step heights and **Clean** case. A similar trend is followed by **Step 2** cases where the small step height **Case 2a** does not have any influence on tripping and has very similar losses compared to the **Clean** case. The tripping effects are very adverse when the step heights are increased resulting in increased losses going from **Case 2b** to **2c**. The effectiveness of the boundary layer tripping step has been estimated based on the total pressure loss coefficient using Eq. (5.1):

$$\text{Pressure loss coefficient} = \frac{P_{\text{total\_1}} - P_{\text{total\_2}}}{P_{\text{total\_1}} - P_{\text{static\_1}}}. \tag{5.1}$$

The inlet parameters $P_{\text{total\_1}}$ and $P_{\text{static\_1}}$ is identical for all these cases since the value has been extracted from the point taken at the mid-span and mid-channel located one chord upstream of the blade passage where the inflow conditions are uniform. Whereas the outlet total pressure $P_{\text{total\_2}}$ is mass averaged along the traverse extracted 20 mm downstream, the profile is estimated for one pitch length and is described in Table 5.

TABLE 5. Stagnation pressure loss estimation for different tripping setup.

Configuration	Pressure loss coefficient
Clean	0.170
Case 1a	0.173
Case 1b	0.176
Case 1c	0.214
Case 2a	0.214
Case 2b	0.187
Case 2c	0.219

The averaged pressure losses in all tripping cases are compared with the **Clean** case in Table 5. It is evident that the losses are identical in **Case 1a** and **Case 1b** whereas the losses increase drastically in **Case 2b**, **2c** compared to **Case 1b** and **1c**. When comparing the tripping effect with respect to the **Clean** case the defined case was not able to improve the aerodynamic losses by tripping the boundary layer. To visualise the losses along the average pitch, traverse the stagnation pressure losses have been estimated for each cell point and are plotted in (Fig. 11). It is evident from (Fig. 11) that the wake losses are increased significantly when the step heights are increased irrespective of the step location whereas the decrease in the step height shows that the effect on losses is comparable with the laminar **Clean** case.

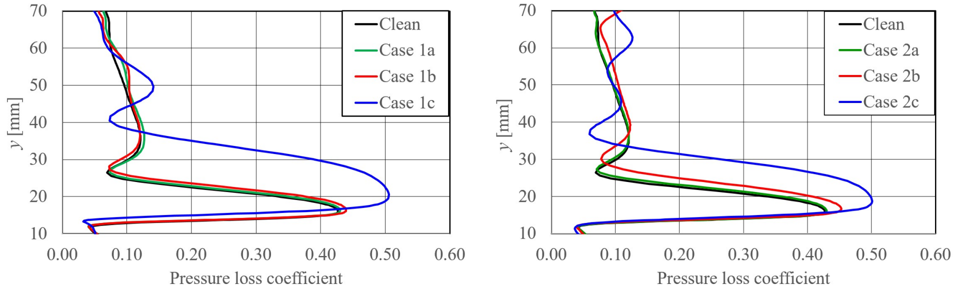

Fig. 11. Comparison of pressure loss coefficient along the pitch traverse downstream the profile (left) **Step 1** cases and (rigth) **Step 2** cases.

6. Conclusions

The paper presents a numerical and experimental investigation of a passive flow control method of boundary layer tripping employing a step on the suction side of a transonic compressor rotor profile. A detailed flow structure comparison has been detailed in this paper which has been carried out on the representative single passage test section for SBLI investigations at the IMP PAN transonic wind tunnel facility. The geometrical size and location of the tripping setup have been defined based on the experimental feasibility of using a tape that was stuck to the suction side of the profile in the test section. The presented numerical results carried out using Numeca/Cadence FINE/Turbo with EARSM turbulence model including transition effects are validated with experimental methods such as surface pressure measurements, schlieren images, and wake measurements. A detailed flow structure investigation was carried out on the suction side of the profile in the test section. Some of the important outcomes are listed:

- It is evident that the boundary layer tripping at ($x/c = 0.16$) has a very minimal effect on tripping the boundary layer to transitional compared to laminar case.
- The differences are more pronounced downstream of the shock interaction where the boundary layer thickness is increased in transitional cases.
- Whereas the leading-edge step over-trips the boundary layer resulting in the thickening of the boundary layer upstream the shock resulting in larger separation and increased losses.
- Also, from the isentropic Mach number and wall shear stress plots, it is evident that shock wave shifts upstream for the turbulent case compared to transitional and laminar configurations.
- Further investigations on the step heights at the chosen cases show the sensitivity of the tripping setup with respect to geometrical definitions and the location at which they are defined on the suction side of the rotor profile.

- The increase of the step height at the transitional case triggers the boundary layer to overtrip whereas the reduction of step height has no effect on the tripping.
- Similarly, in the turbulent case where overtripping was found in experiments the step height reduction shows no effect on tripping, and moreover it tends to have a similar flow structure as a laminar case.
- However, a slight increase shows adverse effects of over-tripping the boundary layer resulting in increased losses compared to laminar and transitional cases.
- RANS model has limitation especially when predicting the separation due to shock interaction or end-wall effect causing corner flows.
- The complex unsteady flow from pressure side of lower profile could also interact with wake and is challenging to capture the wake accurately using LDA measurements.
- Wake measurements close to trailing edge are not ideal due to the lack of seeding at this zone. Whereas further downstream traverse could be affected with mixing of wakes and passage flows.

It could be concluded that the tripping of the boundary layer is sensitive to the step height. The goal of tripping the boundary layer from laminar to transitional SBLI could be achieved with an appropriate geometrical setup. A reduction of shock unsteadiness could be found in the case of turbulent interaction. It could be concluded that an improper geometrical configuration can lead to negative impact on flow characteristics. Therefore, this research contributes to further development of passive flow control methods to achieve higher performance improvement in transonic flow compressors.

Acknowledgements

This research was supported by the 7 EU framework project and was carried out within the research project with the acronym TFAST (Transition Location Effect on Shock Wave Boundary Layer Interaction). This research was supported by CI TASK and PL-Grid Infrastructure.

References

1. H.A. Schreiber, W. Steinert, B. Kusters, *Effects of Reynolds number and free-stream turbulence on boundary layer transition in a compressor cascade*, Journal of Turbomachinery, **124**, 1, 1–9, 2002.
2. H. Alexander, J. Klinner, S. Grund, C. Willert, W. Steinert, M. Beversdorff, *On the importance of transition control at transonic compressor blades*, Journal of Turbomachinery, **143**, 3, 031007, 2021.

3. D. Arnal, J. Delery, *Laminar-turbulent transition and shock wave/boundary layer interaction*, Office National d'Etudes et de Recherches Aérospatiales Onera-publications-tp, **109**, 69, 2004.

4. D.S. Todd, H. Babinsky, *Influence of Transition on the Flow Downstream of Normal Shock Wave-boundary Layer Interaction*, 54th AIAA Aerospace Science Meeting, 2016.

5. G. Patrick, P. Flaszynski, R. Szwaba, M. Piotrowicz, P. Kaczynski, B. Tartinville, C. Hirsch, A. Hergt, *Transition Location Effect on Shock Wave Boundary Layer Interaction: Experimental and Numerical Findings from the TFAST Project*, Notes on Numerical Fluid Mechanics and Multidisciplinary Design, Springer, **144**, 2020.

6. A. Hergt, J. Klinner, J. Wellner, C. Willert, S. Grund, W. Steinert, M. Beversdorff, *The present challenge of transonic compressor blade design*, Journal of Turbomachinery, **141**, 9, 091004, 2019.

7. A. Joseph, P. Flaszynski, P. Doerffer, M. Piotrowicz, *Low Reynolds Number Effect on Highly Loaded Compressor Stator Cascade*, 15th European Conference on Turbomachinery Fluid Dynamics & Thermodynamics European Turbomachinery Society, **239**, 2023.

8. L. Wesley, D.M. Martin, G. Tillman, *Flow control opportunities in gas turbine engines*, Fluids 2000 Conference and Exhibit, 2000.

9. M. Hecklau, C. Gmelin, W. Nitsche, F. Thiele, A.Huppertz, M. Swoboda, *Experimental and numerical results of active flow control on a highly loaded stator cascade*, Proceedings of the Institution of Mechanical Engineers, Part A: Journal of Power and Energy, **225**, 7, 907–918, 2011.

10. M. Bright, D. Culley, E. Braunscheidel, G. Welch, *Closed Loop Active Flow Separation Detection and Control in a Multistage Compressor*, [in:] 43rd AIAA Aerospace Science Meeting and Exhibit, 849, 2005.

11. A. Hegt, R. Meyer, K. Engel. *Experimental investigation of flow control in compressor cascades*, Turbo Expo: Power for Land, Sea and Air, **4241**, 2006.

12. S. Kubacki, Z. Rarata, A. Drozdz, R. Gnatowska, V. Sokolenko, W. Elsner, *Prediction of laminar-to-turbulent transition in a separated boundary layer subjected to an external acoustic forcing*, Archives of Mechanics, **75**, 5, 591–616, 2023.

13. J. Tiainen, A. Gronman, A.J. Varri, J. Backman, *Flow control methods and their applicability in low-Reynolds-number centrifugal compressors-a review*, International Journal of Turbomachinery, Propulsion and Power, **3**, 1, 2, 2018.

14. V. Shinde, J. McNamara, D. Gaitonde, *Control of transitional shock wave boundary layer interaction using structurally constrained surface morphing*, Aerospace Science and Technology, **96**, 105545, 2020.

15. P. Doerffer, O. Szulc, *Shock wave smearing by wall perforation*, Archives of Mechanics, **58**, 6, 543–573, 2006.

16. C. Lietmeyer, B. Denkena, T. Krawczyk, R. Kling, L. Overmeyer, B. Wojakowski, E. Reithmeier, R. Scheuer, T. Vynnyk, J.R. Seume, *Recent advances in manufacturing of riblets on compressor blades and their aerodynamic impact*, Journal of Turbomachinery, **135**, 4, 041008, 2013.

17. N. Tabatabaei, R. Vinuesa, R. Örlü, P. Schlatter, *Techniques for turbulence tripping of boundary layers in RANS simulations*, Flow, Turbulence and Combustion, **108**, 3, 661–682, 2022.

18. P. Doerffer, P. Flaszynski, J.P. Dussauge, H. Babinsky, P. Grothe, A. Petersen, F. Billard [eds.], *Transition Location Effect on Shock Wave Boundary Layer Interaction: Experimental and Numerical Findings from the TFAST Project*, Springer Nature, **144**, 2020.

19. P. Flaszynski, P. Doerffer, R. Szwaba, M. Piotrowicz, P. Kaczynski, *Laminar-turbulent transition tripped by step on transonic compressor profile*, Journal of Thermal Science, **27**, 1, 1–7, 2018.

20. P. Flaszynski, P. Doerffer, R. Szwaba, P. Kaczynski, M. Piotrowicz, *Shock wave boundary layer interaction on suction side of compressor profile in single passage test section*, Journal of Thermal Science, **24**, 510–515, 2015.

21. J. Antony, W. Schmidt, E. Turkel, *Numerical solution of the Euler equations by finite volume methods using Runge Kutta time stepping schemes*, 14th Fluid and Plasma Dynamics Conference, 1981.

22. Numeca FINE$^{\mathrm{TM}}$/Turbo Theoretical Manual Documentation, **17**, 1a, 2022.

23. F.R. Menter, A.V. Garbaruk, Y. Egorov, *Explicit algebraic Reynolds stress models for anisotropic wall-bounded flows*, Progress in Flight Physics, **3**, 89–104, 2012.

24. H. Blasius, *The boundary layers in fluids with little friction*, National Advisory Committee for Aeronautics, **1256**, 1950.

Received April 17, 2024; revised version August 22, 2024.
Published online October 28, 2024.